doi:10.1088/1742-6596/86/1/012011

Ion behavior in capacitively-coupled dual-frequency discharges

Zoltán Donkó

Research Institute for Solid State Physics and Optics, Hungarian Academy of Sciences, H-1525 Budapest, POB 49, Hungary

E-mail: donko@sunserv.kfki.hu

Zoran Lj. Petrović

Institute of Physics, POB 68, Pregrevica 118, 11080 Belgrade-Zemun, Serbia

E-mail: zoran@phy.bg.ac.yu

Abstract. Particle-in-cell (PIC/MCC) simulations of capacitively-coupled Ar, CF_4 , and CF_4 /Ar discharges excited by a single RF source or by two sources of different frequencies are presented. The properties and the formation mechanism of the flux-energy distribution of the ions reaching the electrodes is analyzed in detail. It is demonstrated that at low pressures the ion energy and the ion flux can nearly independently be controlled by properly choosing the excitation frequencies.

1. Introduction

Radio-frequency capacitively coupled plasma (CCP) sources have been widely used in technological steps of modern integrated circuit fabrication [1]. In particular CCPs are applied for etching of the dielectrics, where high ion energies are required [2]. The control of plasma properties in these applications is of primary importance. During the last couple of years it has been recognized that the plasma maintenance and ion properties may be controlled independently from each other using plasma sources excited by two different radio frequencies [3, 4, 5].

In principle one needs to be able to control plasma properties including the flux of ions by the high frequency rf source and to control the energy of the ions by the low frequency rf source. The low frequency source should not turn on and off the plasma or change its properties dramatically. At the same time the high voltages applied in the control of the ion energy mean that the low frequency source may affect the plasma significantly. Additional requirement arises from the need to employ pulsed plasmas, especially in order to reduce the charging damage [6]. It implies that when the high frequency source is off, the low frequency source should not be able to sustain the plasma on its own.

Properties of capacitively coupled radio-frequency discharges driven by two frequencies have been explored with the aid of different models [7, 8, 9, 10, 11]. The flux and energy distribution of the ions interacting with the electrode (target) surfaces is of primary importance. Understanding the details of ion properties is the motivation of the present study, in which we investigate

doi:10.1088/1742-6596/86/1/012011

discharges in Ar, CF₄ and their mixtures, the latter being used in the etching of silicon and silicon-dioxide. One should bear in mind that recently Turner and Chabert [12] have given a deeper understanding of the interaction between the two plasma sources and their effect on the mechanism of electron heating. The present paper, however, focuses on practical issues, the quality (energy and flux) of ions reaching the processed surface. The present numerical model could be employed to make a systematic test of the model of Turner and Chabert but that is beyond the scope of this paper.

2. Model

Symmetrical discharges in Ar, CF₄ and CF₄/Ar excited by a single RF source, or by two RF sources with different frequencies are described here by one-dimensional (1d3v) bounded plasma particle-in-cell simulation, complemented with Monte Carlo treatment of collision processes (PIC/MCC). The electrodes are assumed to be plane and parallel, and separated by a distance of L=2 cm. The gas pressure is fixed at 20 mTorr. The charged species taken into account in the model are CF₃⁺, CF₃⁻, F⁻ and Ar⁺ ions, and electrons. The cross sections of e⁻– CF₄ collision processes are taken from Kurihara *et al.* [13], with the exception of electron attachment processes (producing CF₃⁻ and F⁻ ions) which are taken from Bonham [14]. The cross sections for electron - argon atom interaction are taken from [15]. The electron impact collision processes considered in the model are listed in Table 1.

Table 1. List of electron - CF_4/Ar collisions considered in the model. E_0 is the energy threshold in eV.

Collision partners	Description	Product	E_0
$e^- + CF_4$	Elastic momentum transfer		0
$e^- + CF_4$	Vibrational excitation		0.108
$e^- + CF_4$	Vibrational excitation		0.168
$e^- + CF_4$	Vibrational excitation		0.077
$e^- + CF_4$	Electronic excitation	CF_4^*	7.54
$e^- + CF_4$	Dissociative ionization	CF_3^{++}	41
$e^- + CF_4$	Dissociative ionization	CF_3^+	16
$e^- + CF_4$	Dissociative ionization	CF_2^{++}	42
$e^- + CF_4$	Dissociative ionization	$\mathrm{CF}_2^{\bar{+}}$	21
$e^- + CF_4$	Dissociative ionization	$\mathrm{CF}^{\mathtt{\bar{+}}}$	26
$e^- + CF_4$	Dissociative ionization	C^+	34
$e^- + CF_4$	Dissociative ionization	F^{+}	34
$e^- + CF_4$	Attachment	F^-	0
$e^- + CF_4$	Attachment	CF_3^-	0
$e^- + CF_4$	Neutral dissociation	CF_3	12
$e^- + CF_4$	Neutral dissociation	CF_2	17
$e^- + CF_4$	Neutral dissociation	CF	18
$e^- + Ar$	Elastic momentum transfer		0
$e^- + Ar$	Electronic excitation	Ar^*	11.5
$e^- + Ar$	Ionization	Ar^{+}	15.8

For ion-molecule reactions reactive, as well as elastic collisions are considered [16, 17]. Ar⁺ + Ar collisions are treated as given by Phelps [18]. For the elastic collisions of ions with buffer

doi:10.1088/1742-6596/86/1/012011

gas atoms and/or molecules (other than $Ar^+ + Ar$) Langevin cross sections are used:

$$\sigma_{\rm L} = \left(\frac{\pi \alpha_{\rm p} e^2}{\varepsilon_0 \mu}\right)^{1/2} \beta_{\infty}^2 g^{-1},\tag{1}$$

where μ is the reduced mass, $\alpha_{\rm p}$ is the polarizibility, g is the relative velocity and β_{∞} is the dimensionless impact parameter for which the deflection angle is negligible [16].

Recombination processes between positive and negative ions, as well as between electrons and CF_3^+ ions are simulated according to the procedure given by Nanbu and Denpoh [19]. The ion-ion recombination rate coefficients are taken from Rauf and Kushner [20], while the rate of electron - CF_3^+ recombination process is from Denpoh and Nanbu [21]. The effect of the recombination rates on the simulation results was studied in [22]. This study has concluded that the electron-ion $(CF_3^+ + e^-)$ recombination rate has relatively little influence on CF_3^+ ion density, since the rate of CF_3^+ creation through ionization vastly exceeds the rates of recombination processes, i.e. the major part of CF_3^+ ions is lost at the electrodes. This statement also holds for the electrons, as the e-i recombination has a low rate. On the other hand, the increase of the ion-ion recombination rate coefficients was found to result in a significant decrease of the ion densities, especially in discharges in pure CF_4 .

The ion-molecule reactions and recombination processes considered in our model are listed in Tables 2 and 3, respectively.

Table 2. In - molecule collisions considered in the model. E_0 is the energy threshold in eV.

Projectile	Reaction	E_0
CF_3^+	$CF_3^+ + CF_4 \rightarrow CF_2^+ + CF_4 + F$	5.843
CF_3^+	$CF_3^+ + CF_4 \rightarrow CF_3^+ + CF_3 + F$	5.621
CF_3^+	$CF_3^+ + CF_4 \rightarrow CF_3^+ + CF_4$	0
CF_3^+	$CF_3^+ + Ar \rightarrow CF_3^+ + Ar$	0
CF_3^-	$\mathrm{CF_3^-} + \mathrm{CF_4} \to \mathrm{CF_4} + \mathrm{CF_3} + \mathrm{e^-}$	1.871
CF_3^-	$CF_3^- + CF_4 \rightarrow CF_3^- + CF_3 + F$	5.621
CF_3^-	$\mathrm{CF}_3^- + \mathrm{CF}_4 \to \mathrm{CF}_2^- + \mathrm{CF}_4 + \mathrm{F}^-$	1.927
CF_3^-	$CF_3^- + CF_4 \rightarrow CF_3^- + CF_4$	0
CF_3^-	$CF_3^- + Ar \rightarrow CF_3^- + Ar$	0
F-	$F^- + CF_4 \rightarrow CF_4 + F + e^-$	3.521
F^-	$F^- + CF_4 \rightarrow CF_3 + F^- + F$	5.621
F^-	$F^- + CF_4 \rightarrow F^- + CF_4$	0
F^-	$F^- + Ar \rightarrow F^- + Ar$	0
Ar^+	$Ar^+ + Ar \rightarrow Ar^+ + Ar \text{ (isotropic)}$	0
Ar^{+}	$Ar^+ + Ar \rightarrow Ar^+ + Ar$ (backscattering)	0
Ar ⁺	$Ar^+ + CF_4 \rightarrow Ar^+ + CF_4$	0

In our simulations we assume $T=300~\mathrm{K}$ temperature for the gas, and do not consider secondary emission and reflection of electrons from the electrodes. Electron-electron Coulomb collisions are described by the method given by Nanbu [23].

doi:10.1088/1742-6596/86/1/012011

Table 3. Recombination processes considered in the model. (The ion and electron temperatures, $T_{\rm i}$ and $T_{\rm e}$, respectively, are given in electronvolts.)

Reaction	Rate coefficient (m ³ s ⁻¹)
$\begin{array}{c} CF_3^+ + e^- \\ CF_3^+ + F^- \\ CF_3^+ + CF_3^- \\ Ar^+ + F^- \\ Ar^+ + CF_3^- \end{array}$	$3.95 \times 10^{-15} T_{\rm i}^{-1} T_{\rm e}^{-0.5}$ 10^{-13} 10^{-13} 10^{-13} 10^{-13}

3. Results

For all the results presented here, in the cases of single frequency excitation the frequency is chosen to be 100 MHz, the same value is applied as "high-frequency" $f_{\rm HF}$ in cases of dual frequency excitation, in accordance with the conditions for optimum functional separation as found by Kitajima and coworkers [3]. The amplitude of the high-frequency is $V_{\rm HF}=60$ V, for all the results.

Spatial distributions of the charged particles are displayed in Fig. 1 for single/dual-frequency excited discharges in argon (a,b), CF_4 (c,d), and 90% Ar + 10% CF_4 (e,f).

Let us first consider the case of single frequency excitation ($V_{\rm LF}=0$). In case of argon buffer gas – see figure 1(a) – the simulation reproduces the well-known features of electropositive RF discharges: we can observe the formation of ion sheaths near the electrodes and the presence of a quasi-neutral plasma in the center of the discharge gap. In case of CF₄ buffer gas an electronegative discharge is formed, in the bulk plasma the density of negative (F⁻) ions exceeds the electron density by a large factor, as shown in figure 1(c). This observation agrees with experimental findings [24]. The negative ions are strongly confined inside the bulk plasma and their density in the sheaths becomes negligible. In the discharge operated in 90% Ar + 10% CF₄ the bulk plasma is composed mainly of Ar⁺ and F⁻ ions, but the electron density becomes significant, too. CF₃⁺ and CF₃⁻ ions are present in a small concentration in the bulk, the density of CF₃⁺ ions in the sheath is ≈ 10 % of that of the Ar⁺ ions. When the low-frequency excitation with $f_{\rm LF}=1$ MHz is applied, we observe, as general trends, (i) a reduction of the charged particle density and (ii) an increase of the width of the sheaths. The density ratios of the different ions (in the case of CF₄-containing discharges) do not change significantly (see figure 1).

In the following we analyze the flux-energy distribution of the positive ions reaching the electrodes (see figure 2). At single frequency operation, $V_{\rm LF}=0$, the distributions sharply peak for both the pure gases and for the 90% Ar + 10% CF₄ gas mixture at the energy $\varepsilon\approx 40$ eV, the time-averaged value of the sheath potential. At $V_{\rm LF}>0$ the distributions extend towards higher energies, and exhibit a characteristic saddle shape. At the pressure of 20 mTorr the ion transit time is shorter than $1/f_{\rm LF}$, and, as the sheaths are nearly collisionless, the energy of ions reaching the electrodes at a given time strongly correlates with the difference of the instantaneous plasma potential and the potential of the powered electrode. There is only one marked difference between the flux-energy distributions of Ar⁺ and CF₃⁺ ions: while a significant number of low energy Ar⁺ ions arrive at the electrodes, the energy spectrum of CF₃⁺ ions cuts off towards zero ion energy.

This difference can be explained by the following. (i) Above ≈ 1 eV energy the cross section of $CF_3^+ + CF_4$ collisions becomes lower than the cross section of the $Ar^+ + Ar$ (symmetric) collisions (see figure 3). Thus CF_3^+ ions traverse the sheaths experiencing a lower number of collisions, which would result in energy loss. (ii) Although the (Langevin) cross sections for

doi:10.1088/1742-6596/86/1/012011

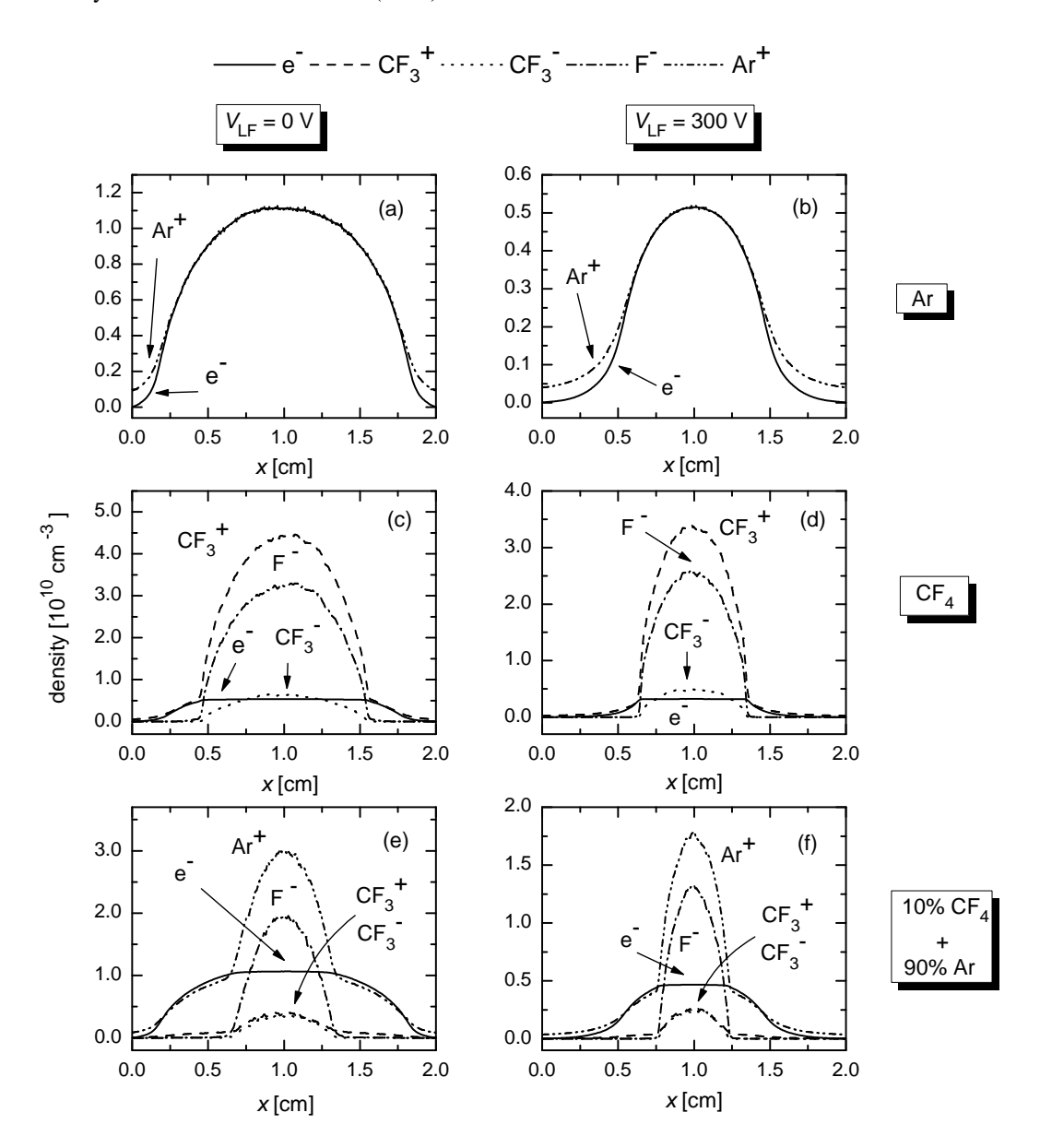


Figure 1. Distributions of charged particle densities for 100 MHz single-frequency (left column) and 100 MHz / 1 MHz dual-frequency (right column) discharges. The buffer gas is Ar for (a) and (b), CF₄ for (c) and (d), and 90% Ar + 10% CF₄ for (e) and (f). The gas pressure is 20 mTorr for all cases and $V_{\rm LF} = 300$ V for dual-frequency driven discharges. $V_{\rm HF} = 60$ V.

the CF_3^+ + Ar and the Ar^+ + CF_4 processes are nearly the same, CF_3^+ ions are deflected in a smaller extent due to their greater mass.

The effect of $f_{\rm LF}$ on the flux-energy distributions of the CF₃⁺ and Ar⁺ ions is illustrated in figure 4. It can be seen that for Ar⁺ ions multiple peaks appear in the energy spectrum at $f_{\rm LF} > 1$ MHz, which is a consequence of the combined effects of charge exchange collisions in the sheaths and the repeated acceleration of the ions flying from the bulk plasma to the electrodes [25]. The appearance of these peaks have already been analyzed in details both in the casees of single- and dual-frequency excitation. At $f_{\rm LF} > 1$ MHz the ion transit time through the sheath becomes greater than $1/f_{\rm LF}$, i.e. the ions cross the sheath during a couple to several

doi:10.1088/1742-6596/86/1/012011

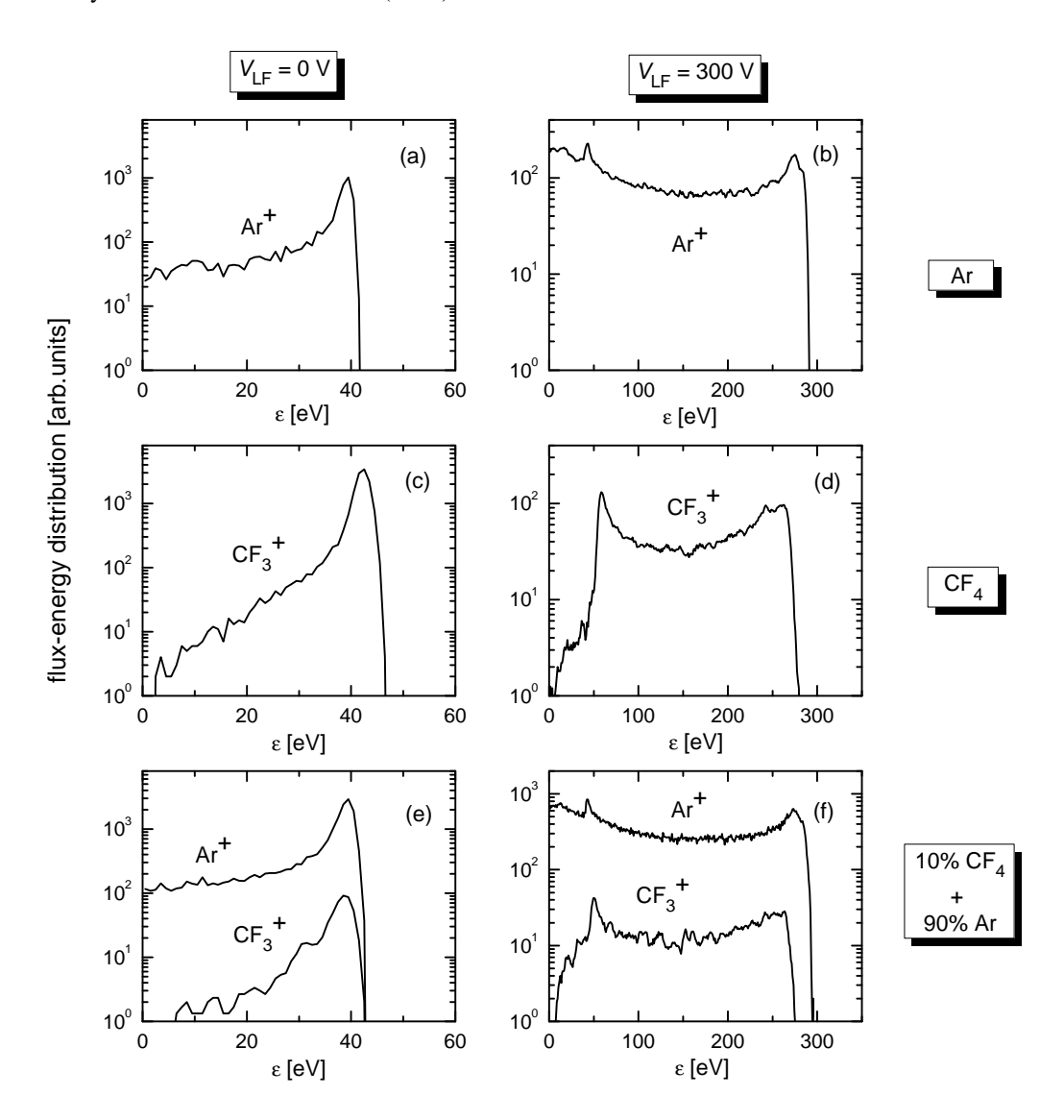


Figure 2. Flux-energy distributions of CF_3^+ and Ar^+ ions at the electrodes for 100 MHz single-frequency (left column) and 100 MHz / 1 MHz dual-frequency (right column) discharges. The buffer gas is Ar for (a) and (b), CF_4 for (c) and (d), and 90% Ar + 10% CF_4 for (e) and (f). The gas pressure is 20 mTorr and $V_{LF} = 300$ V for dual-frequency driven discharges. $V_{HF} = 60$ V.

low-frequency cycles. For the CF_3^+ ions we observe that the distributions get more peaked at the highest energies when f_{LF} is increased.

The formation of the distributions shown in figure 2(f) is further analyzed in figure 5. Figures 5(a), (b) and (c), respectively, display the excitation voltage of the powered electrode, the calculated plasma potential, and the voltage drop over the electrode sheath, over a single period of the low-frequency excitation. Figures 5(d), (e) and (f), respectively, display the the joint temporal and energy distribution of electrons, Ar^+ ions, and CF_3^+ ions arriving at the powered electrode. Dots on the energy - time plane of these latter panels of figure 5 correspond to individual electrons / ions reaching the powered electrode. The data for the $100 \, \text{MHz} / 1 \, \text{MHz}$ discharge at $20 \, \text{mTorr}$ clearly show that the energy of most of the positive ions at the powered electrode follows the difference between the plasma potential and the instantaneous value of the

doi:10.1088/1742-6596/86/1/012011

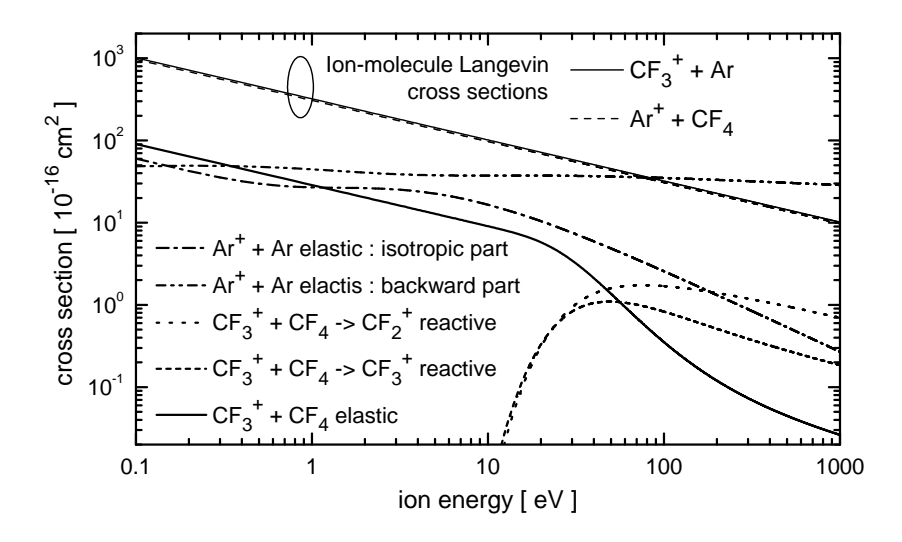


Figure 3. Cross sections of CF_3^+ and Ar^+ ions in CF_4 + Ar gas mixture. The CF_3^+ + CF_4 cross sections and data for the calculation of the Langevin cross sections (calculated using $\beta_{\infty} = 3$ in Eq. (1)) are taken from Georgieva *et al.* [16]; data for Ar^+ + Ar collisions are from Phelps [18].

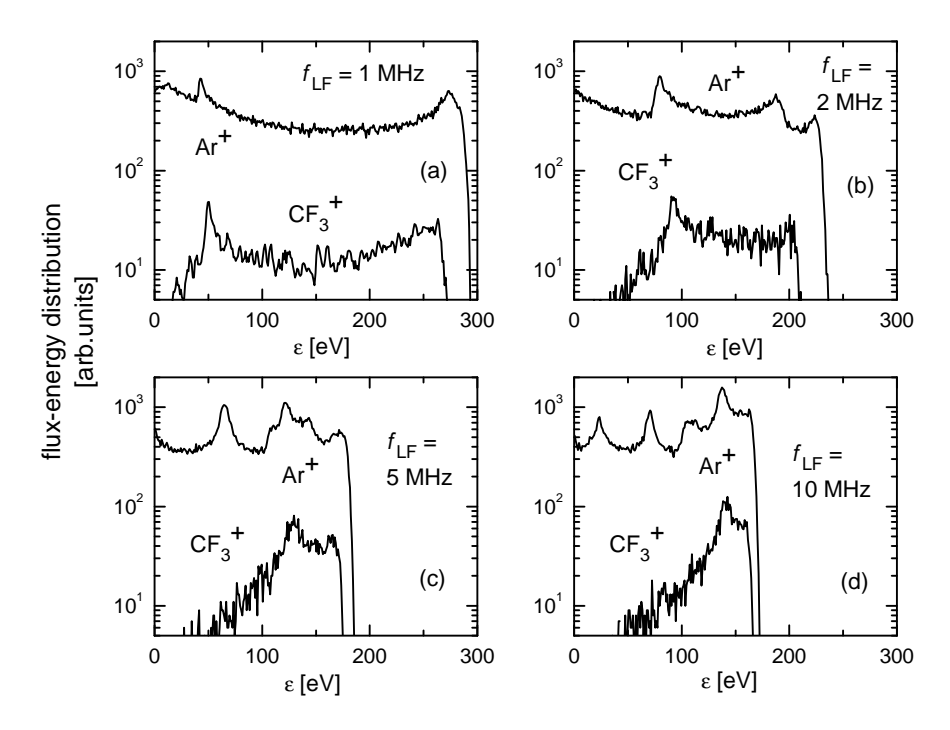


Figure 4. Effect of the value of the lower excitation frequency $f_{\rm LF}$ on the flux-energy distributions of CF₃⁺ and Ar⁺ ions at the electrodes. $f_{\rm HF}=100$ MHz, $V_{\rm HF}=60$ V, and $V_{\rm LF}=300$ V.

applied excitation voltage (i.e. the sheath voltage). We observe a "phase shift" between the energy distribution of the ions and the accelerating voltage (the highest ion energies are observed subsequent to the occurrence the maximum of the accelerating potential). This delay originates from the finite ion transit time through the sheath. In the case of the above discharge conditions

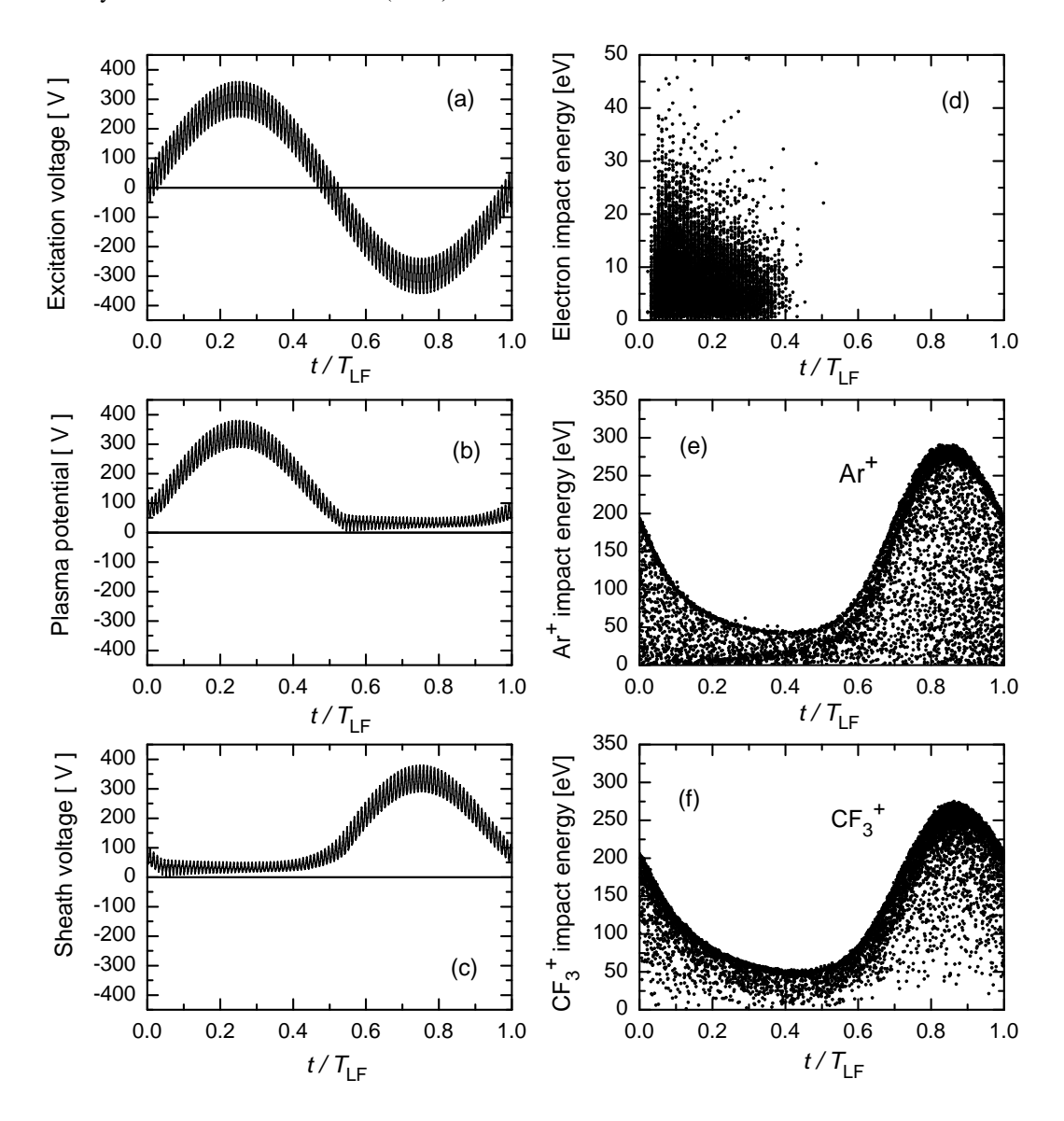


Figure 5. (a) Excitation voltage, (b) calculated plasma potential, and (c) sheath voltage in a 10% CF₄ + 90% Ar discharge, over a single cycle of the low-frequency excitation. (d), (e), (f): spatiotemporal distribution of the flux and energy of electrons, Ar⁺ ions, and CF₃⁺ ions, respectively. Dots in these plots correspond to individual particles arriving at the powered electrode. Discharge conditions: p = 20 mTorr, $f_{\rm HF} = 100$ MHz @ $V_{\rm HF} = 60$ V, and $V_{\rm LF} = 300$ V @ $f_{\rm LF} = 1$ MHz.

many of the ions acquire the highest possible energy (the dots are concentrated at the envelope of the distribution shown in figures 5(e) and (f), especially for (f)), although we observe ions with lower energies as well, in accordance with the corresponding flux-energy (time-integrated) distribution displayed in figure 2(f).

So far we have observed that the flux-energy distribution of the ions can be tuned by the low-frequency voltage. In figure 6 it is demonstrated that this can be achieved at a nearly constant flux of the ions when $V_{\rm HF}$ is fixed. Following an initial small decrease the flux of ions remains nearly constant when the low-frequency voltage is increased. Meanwhile, the average

doi:10.1088/1742-6596/86/1/012011

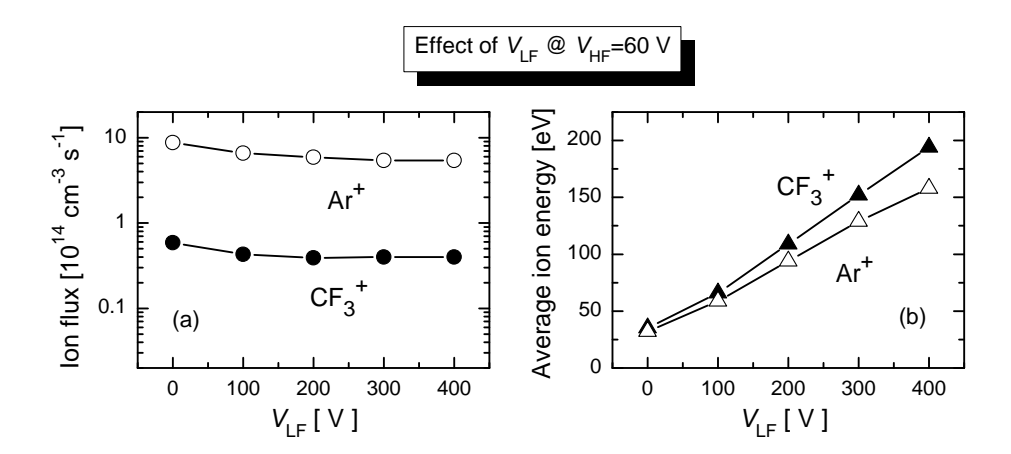


Figure 6. Effect of the low-frequency voltage amplitude on ion properties: (a) ion flux and (b) average energy of ions reaching the electrodes, in 100 MHz / 1 MHz discharges at fixed $V_{\rm HF} = 60$ V. Open symbols: Ar⁺, filled symbols: CF₃⁺. p = 20 mTorr.

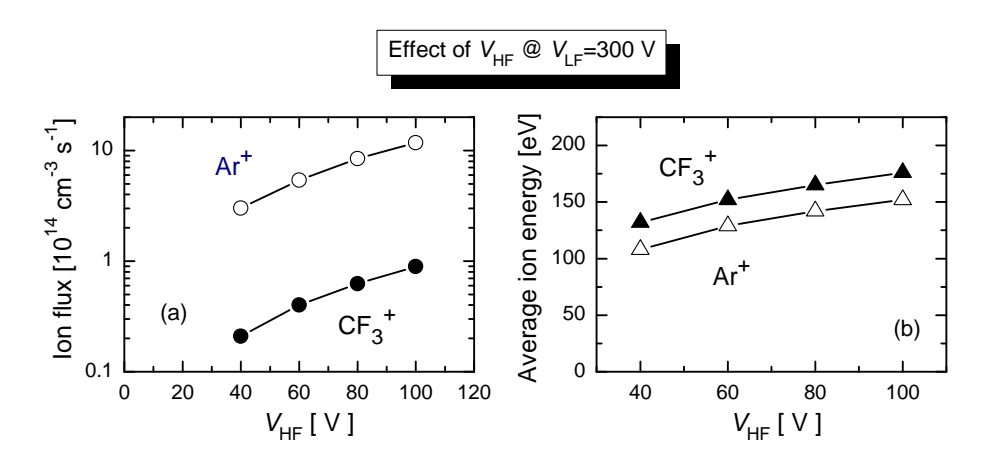


Figure 7. Effect of the high-frequency voltage amplitude on ion properties: (a) ion flux and (b) average energy of ions reaching the electrodes, in 100 MHz / 1 MHz discharges at fixed $V_{\rm LF} = 300$ V. Open symbols: Ar⁺, filled symbols: CF₃⁺. p = 20 mTorr.

energy of the positive ions increases considerably, as displayed in figure 6(b). The flux of the ions (and their density in the bulk plasma, too), on the other hand, can be controlled by the high-frequency voltage, as illustrated in figure 7. We observe a nearly linear increase of the ion fluxes with increasing $V_{\rm HF}$, whereas the average energy of ions changes only slightly. These observations confirm that the dual-frequency excitation, when operating conditions are properly chosen, makes it possible to realize a nearly independent control of the ion energy and flux in low-pressure plasma sources.

Acknowledgments

This work has been supported by the Hungarian Scientific Research Fund through the grant OTKA-T-48389 and also by projects 141025, MNZZS of Serbia and EU-COE project INCO-CT-2006-026328 - IPB-CNP.

doi:10.1088/1742-6596/86/1/012011

References

- [1] Liberman M A and Lichtenberg A J 1994 Principles of Plasma Discharges and Materials Processing (Wiley & Sons, New York)
- [2] Makabe M and Petrović Z Lj 2006 Plasma Electronics: Applications in Microelectronic Device Fabrication (Taylor and Francis, CRC Press, New York)
- [3] Kitajima T, Takeo Y, Petrović Z LJ and Makabe T 2000 Appl. Phys. Lett. 77 489
- [4] Fujita T and Makabe T 2002 Plasma Sources Sci. Technol. 11 142
- [5] Denda T, Miyoshi Y, Komukai Y, Goto T, Petrović Z LJ and Makabe T 2004 J. Appl. Phys. 95 870
- [6] Ohmori T, Goto T K, Kitajima T and Makabe T 2003 Appl. Phys. Lett. 83 4637
- [7] Robiche J, Boyle P C, Turner M M and Ellingboe A R 2003 J. Phys. D 36 1810
- [8] Wakayama G and Nanbu K 2003 IEEE Trans. Plasma Sci. 31 638
- [9] Kim H C and Lee J K 2005 J. Vac. Sci. Technol. A 23 651
- [10] Salabas A and Brinkmann R P 2005 Plasma Sources Sci. Technol. 14 S53
- [11] Donkó Z and Petrović Z Lj 2006 Jpn. J. Appl. Phys. 45 8151
- [12] Turner M M and Chabert P 2006 Phys. Rev. Lett. 96 205001
- [13] Kurihara M, Petrović Z Lj and Makabe T 2000 J. Phys. D 33 2146
- [14] Bonham R A 1994 Jpn. J. Appl. Phys. 33 4157
- [15] Phelps A V http://jilawww.colorado.edu/research/colldata.html
- [16] Georgieva V, Bogaerts A and Gijbels R 2003 J. Appl. Phys. 93 2369; 2003 J. Appl. Phys. 94 3748; 2004 Phys. Rev. E 69 026406
- [17] Nanbu K 2000 IEEE Trans. Plasma Sci. 28 971
- [18] Phelps A V 1994 J. Appl. Phys. **76** 747
- [19] Nanbu K and Denpoh K 1998 J. Phys. Soc. Jpn. 67 1288
- [20] Rauf S and Kushner M J 1997 J. Appl. Phys. 82 2805
- [21] Denpoh K and Nanbu K 2000 Jpn. J. Appl. Phys. 39 2804
- [22] Donkó Z, Petrović Z Lj and Booth J P 2006 Proc. of 23rd Summer School and International Symposium on Physics of Ionized Gases (August 28 - September 1, 2006, Kopaonik, Serbia) p. 399
- [23] Nanbu K 1997 Phys. Rev. E 55 4642, 2000 IEEE Trans. Plasma Sci. 28 971
- [24] Haverlag M, Kono A, Passchier D, Kroesen G M W, Goedheer W J and de Hoog F J 1991 J. Appl. Phys. 70 3472:
- [25] Liu J, Huppert G L and Sawin H H 1990 J. Appl. Phys. 68 3916 Wild C and Koidl P 1991 J. Appl. Phys. 69 2909; Lee J K, Manuilenko O V, Babaeva N Yu, Kim H C and Shon J W 2005 Plasma Sources Sci. Technol. 14 89